Phase decomposition in the Ni–InGaAs system at high annealing temperature

N. Oueldna, Carine Perrin-Pellegrino, Alain Portavoce, Philippe Rodriguez, L. Bih, A. Bouayad, Khalid Hoummada

▶ **To cite this version:**

N. Oueldna, Carine Perrin-Pellegrino, Alain Portavoce, Philippe Rodriguez, L. Bih, et al.. Phase decomposition in the Ni–InGaAs system at high annealing temperature. Journal of Materials Science, 2023, 58 (40), pp.15738-15747. 10.1007/s10853-023-09037-7 . hal-04537629

HAL Id: hal-04537629

https://cnrs.hal.science/hal-04537629v1

Submitted on 8 Apr 2024

HAL is a multi-disciplinary open access archive for the deposit and dissemination of scientific research documents, whether they are published or not. The documents may come from teaching and research institutions in France or abroad, or from public or private research centers.

L'archive ouverte pluridisciplinaire **HAL**, est destinée au dépôt et à la diffusion de documents scientifiques de niveau recherche, publiés ou non, émanant des établissements d'enseignement et de recherche français ou étrangers, des laboratoires publics ou privés.

Distributed under a Creative Commons Attribution - NonCommercial - NoDerivatives 4.0 International License

Phase decomposition in the Ni-InGaAs system at high annealing temperature

N. Oueldna[1,2,*], C. Perrin-Pellegrino[1], A. Portavoce[1], Ph. Rodriguez[3], L. Bih[4], A. Bouayad[4] and K. Hoummada[1,*].

[1]*IM2NP, Aix Marseille Univ/CNRS, UMR 7334, 13397, Marseille, France*

[2]*Applied Chemistry and Engineering Research Centre of Excellence (ACER CoE), Mohammed VI Polytechnic University, Lot 660, Hay Moulay Rachid, Ben Guerir 43150, Morocco*

[3]*Univ. Grenoble Alpes, CEA, LETI, F-38000 Grenoble, France*

[4]*Laboratory of Sciences and Crafts of Engineer, Materials and Processes Department, ENSAM-Meknes, Moulay Ismail University, Meknes, Morocco*

Abstract

III-V semiconductor compounds are increasingly attracting attention as promising candidates for serving as channel materials, especially in the development of contact recovery for sub-10 nm metal-oxide-semiconductor field-effect transistor (MOSFETs) devices or photonic applications. To contribute to this research, the Ni-InGaAs contact was formed by a solid-state reaction between Ni and a $(In_{0.53}Ga_{0.47})As$ layer after heat treatment at 550 °C by a rapid thermal annealing. Atom Probe Tomography (APT) analyses were carried out to study the distribution of elements in the intermetallic phases formed. It was found that at this high temperature, an As-rich phase and a Ga-rich phase are formed simultaneously. The co-existence of these two new phases reveals the occurrence of chemical diffusion and decomposition processes at the Ni-InGaAs interface. These results provide insights into the formation of the As-rich and Ga-rich phases within the quaternary (Ni-Ga-As-In) system upon annealing at 550 °C.

Keywords: Ni/InGaAs contact, atom probe tomography, solid-state reaction, diffusion and grain boundaries.

*Corresponding authors: nouredine.oueldna@um6p.ma (N. Oueldna), khalid.hoummada@im2np.fr (K. Hoummada).

Introduction

Today's microelectronic devices, particularly MOSFETs, rely heavily on silicon substrate. In fact, most research into improving MOSFETs devices focuses on shrinking the transistor dimensions to improve the performance of the final device. However, once a certain dimension is reached, typically below 10 nm, it becomes increasingly difficult to ensure the quality of the device [1]. In fact, tunneling effects due to extreme channel size and overheating due to power consumption become increasingly difficult to control [2]. One solution, among others, is to replace silicon with III-V materials as the channel material [3,4]. III-V compounds are envisaged for a wide range of microelectronic applications such as advanced complementary metal-oxide-semiconductor (CMOS) devices [5], high-speed heterojunction bipolar transistors (HBTs) [6] and High Electron Mobility Transistors (HEMTs) [7]. In optoelectronics, III-V materials are widely used for laser [8] and photodetector [9] applications. These materials offer an interesting mobility of the charge carriers and thus allow the use of less powerful devices, delaying the need to go to very small dimensions [1,10–12]. Among these compounds, $In_{0.53}Ga_{0.47}As$ (referred as InGaAs for simplicity) substrates have been chosen for their lattice match with InP. To successfully integrate the InGaAs system, several fabrication steps of MOSFETs have been proposed. Among these steps, the contacts on the source and drain are of utmost importance to ensure a functional device [13,14]. These contacts can be made by the reaction between a metal thin film and an InGaAs layer in a similar way to the silicide formation [15,16]. They must therefore be reproducible, ultra-thin, and result in low resistivity (below 10^{-9} $\Omega \cdot cm^2$). Metallization of InGaAs by Ni has been widely investigated in recent years in thin films [17–23] and nanowire

configuration [24], especially mainly because of its high electrical performance [10,25–28]. The selected compounds should be stable after high temperatures annealing around 550 °C to ensure efficient electrical contact during device operation.

The results obtained by several research groups interested in the metallization of InGaAs by Ni thin films have revealed many reactions between these components. In fact, Ivana *et al.* [17] have shown that when 28 nm of Ni is deposited on InGaAs, a solid-state reaction occurs after a rapid thermal annealing up to 250 °C. The intermetallic formed was reported to be $Ni_4InGaAs_2$. Similarly, Shekhter *et al.* [18] showed that the phase formed at 200 °C was $Ni_2InGaAs$. Thus, Atom Probe Tomography (APT) was used to directly measure the composition of the intermetallic formed at low annealing temperatures (at 350 °C), showing the formation of $Ni_3InGaAs$ as the first and only phase [29]. The formation of $Ni_3InGaAs$ as the first phase has been confirmed by synchrotron 3D-Reciprocal Space Mapping (RSM) technique at similar annealing conditions [30,31].

However, the technological requirements for both front-end and back-end process steps after contact formation tend to consume a significant thermal budget [32,33]. It is therefore important to assess the stability of the Ni-InGaAs phase formed beyond 400°C. In fact, research on a similar reaction between Ni and GaAs shows that there is phase decomposition in NiAs and NiGa beyond 400 °C [34]. Using 3D RSM, it has been shown that the $Ni_2In_{0.53}Ga_{0.47}As$ phase is formed immediately after the $Ni_3(InGa)_{0.5}As$ phase after an annealing at 400°C, followed by the formation of the stable NiAs phase [30]. According to these results, it is likely that there are other phases that are formed at high temperature, and to characterizing them by X-ray diffraction, has been challenging because the phases present in the ternary systems (Ga-In-Ni [35], Ga-Ni-As [36], In-Ni-As [37]) are mostly crystallized in similar B8 structures. Thus, the stability and the

transformation mechanisms of the $Ni_2InGaAs$ phase or $Ni_3InGaAs$ on InGaAs at high temperature are not well known and understood yet.

Herein, the solid-state reaction between Ni thin film and InGaAs at high annealing temperature (550 °C) was investigated by the atom probe tomography (APT) and electron microscopy. These results were discussed based on Ni-Ga-As phase diagrams.

Materials and methods

An 80 nm-thick Ni layer was deposited by physical vapor deposition (PVD, magnetron sputtering) on a Zn-doped InGaAs thin epitaxial layer (< 300 nm) which was grown on a semi-insulating (001) InP substrate. The substrate was cleaned using a 30 s wet process in dilute $HCl:H_2O$=1:2 solution followed by an Ar plasma treatment prior to the Ni deposition process. A 7 nm-thick TiN film was deposited at 100°C on the top of the sample to protect the Ni film from the atmospheric contamination. The capping process was performed in another chamber of the same sputtering setup under vacuum (10^{-8} mbar) and without breaking it. Finally, a rapid thermal annealing was applied under N_2 atmosphere for 1 min at 550 °C to form the contact. Needle-shaped APT tips were prepared using a dual-beam scanning electron microscopy/focused ion beam (SEM/FIB) system after the deposition of a protective layer of Pt above the existing TiN layer. APT analyses were performed in a LEAP 3000X HR instrument. The laser pulse rate was maintained at 100 kHz, and the detection rate was kept to 0.002 event/pulse by increasing the applied voltage. The specimen temperature and the laser energy were set to 20 K and 0.02 nJ, respectively. The data reconstruction, visualization, and analyses were performed using the commercial software IVAS 3.6.8.

Results

The phases formed between the 80 nm-thick Ni film and InGaAs after annealing at 550 °C were analyzed by APT to determine their chemical composition. In fact, APT is a well-known technique that reveals nano-chemistry in 3D down to the near-atomic scale with a chemical resolution of tens of parts-per-million of all the elements that make up the sample being analyzed [38]. Figure 1(a) shows a 52°-tilted scanning electron microscopy (SEM) image of an intermediate step in the preparation of a needle-shaped tip. Under the TiN layer, we can see the presence of two different contrasts corresponding to two phases (α-phase and β-phase). Both final tips used for APT characterization are shown in yellow in this figure. Figure 1(b) shows a reconstructed APT volume ($40 \times 40 \times 70$ nm^3) of the contact in which Ni, As, Ga and In atoms are represented by green, blue, yellow and red dots, respectively. This APT volume shows a homogeneous distribution of β-phase atoms. Figure 1(c) shows another reconstructed APT volume ($60 \times 60 \times 70$ nm^3), which shows an inhomogeneous distribution of all atoms suggesting the presence of two phases. The chemical compositions of these phases were deduced from the mass spectrum, in which no mass overlap was found. A one-dimensional composition profile was calculated in a cylinder perpendicular to the interface between the two observed phases and is plotted in Figure 1(d). Thus, two phases are identified and -labeled up as α-phase and β-phase in Figure 1(c).

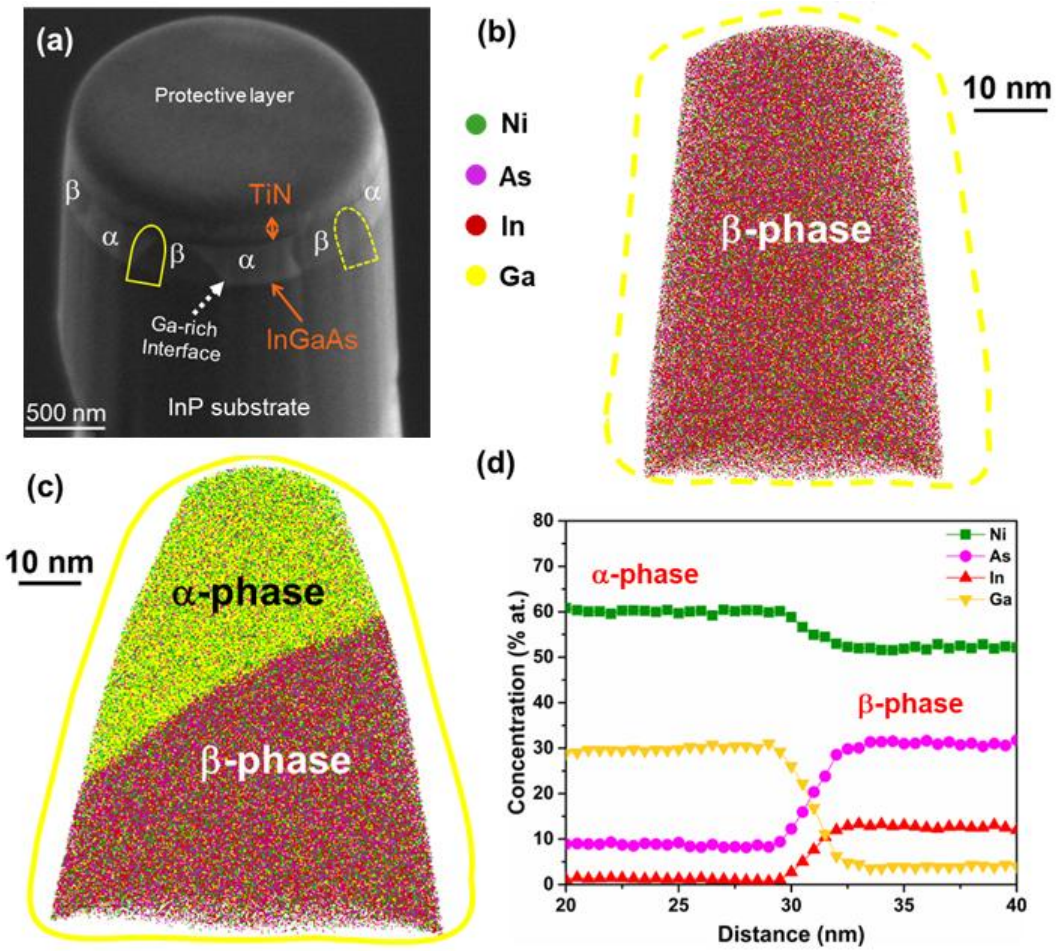

Fig 1. *Results of the APT analysis of the contact after a 550 °C annealing. (a) Scanning electron microscope (SEM) image of an intermediate step during the preparation of the APT tips, showing the presence of the two α- and β-phases. (b) Analyzed volume in 3D showing the β-phase. (c) Analyzed volume in 3D showing the two different α-phase and β-phase. (d) Concentration profiles through a cylinder perpendicular to the α-phase and β-phase interface.*

The average contents of Ni, In, Ga and As in the α-phase are 62.5 ± 0.5, 1.3 ± 0.5, 27.2 ± 0.3, and 9.0 ± 0.6 at%, respectively. For the β-phase, the average chemical composition is 52.1 ± 0.5 % Ni, 12.7 ± 0.2% In, 4.2 ± 0.3% Ga, and 31.0 ± 0.4% As, indicating that the α-phase corresponds to an intermetallic highly enriched in Ga while the β-phase corresponds to a phase highly

enriched in As. For the α-phase, indium is almost completely rejected, changing from a concentration of 11.0 % in $Ni_3(InGa)_{0.5}As$ to 1.3% [29,30].

The atomic concentration was checked by another APT tip, and it was found that the chemical composition of β-phase is almost the same as can be seen in Figure 2.

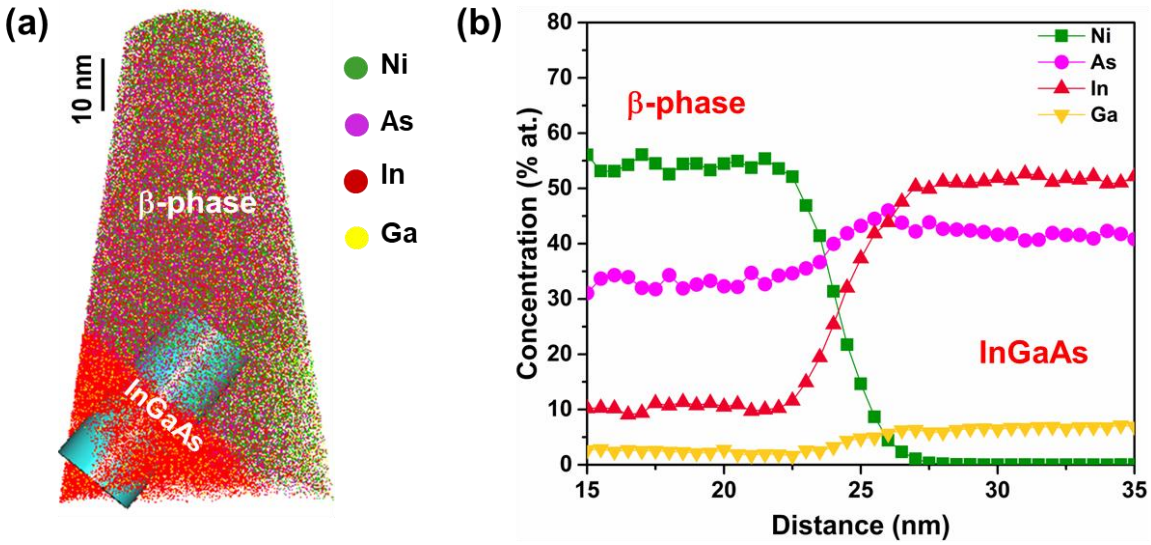

Fig 2. *Results of the APT analysis of the contact after a 550 °C annealing. (a) Analyzed volume in 3D showing the β-phase. (b) concentration profiles through the interface β-phase/InGaAs (cylinder presented in (a)).*

Figure 2(a) shows the analyzed volume in 3D where the cylinder on the left represents the volume over which the integrated concentrations of the elements were calculated. The concentration fractions are 52.5 ± 0.5 % Ni, 12.0 ± 0.7% In, 3.8 ± 0.3% Ga, and 31.7 ± 0.4% As. Figure 2 also shows that the β-phase is in contact with the remaining InGaAs layer at 550 °C. This layer is highly enriched in indium (50% instead of 26,5%), which could be explained by the rejection of indium from the α-phase to the InGaAs layer.

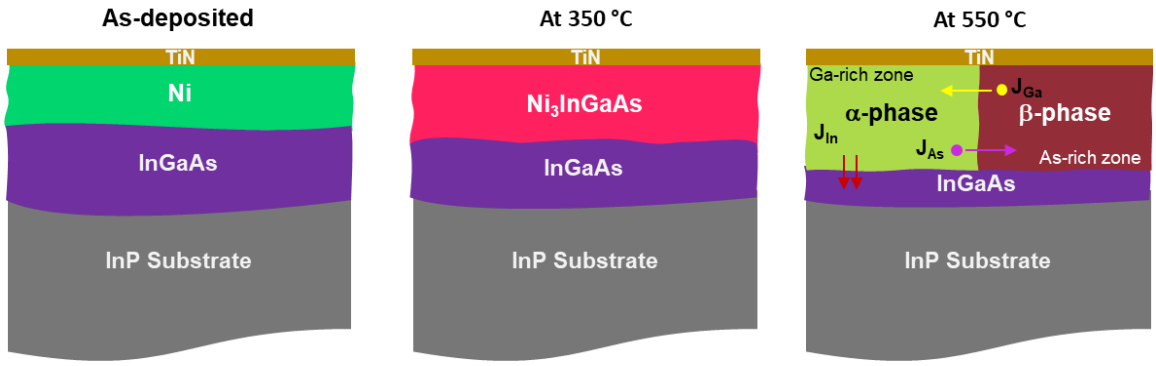

Fig 3. *Schematic illustrations of the stacks in the sample as-deposited and after the solid-state reaction at 350 °C and 550 °C. Atomic redistribution is represented by the atoms flux* J_i.

Figure 3 shows schematic illustrations of the contact as-deposited and after the annealing at 350 °C as previously reported by Perrin *et al.* [29] and at 550 °C with the proposed atomic redistribution between the α-, β-phases and the InGaAs layer. We assume that In is rejected from the α-phase to the InGaAs layer, since its concentration in the β-phase seems to be limited to about ten percent. In the α-phase, As atoms are still present, but they are almost three times less numerous than Ga. Considering that In atoms substitute Ga atoms, the phase would then correspond to $Ni_3(Ga_{1.5}As_{0.5})$. From Figure 1(d) the Ga content in β-phase (4.2%) is much lower compared to the Ga content in the α-phase (27.2%). The As amount is important (31%), the In is also present in β-phase (12.7%), and as a result β-phase corresponds to a $Ni_2(In_{0.52}Ga_{0.16}As_{1.32})$. Consequently, we can consider both α- and β-phases as Ni(Ga-rich) and Ni(As-rich) phases, respectively. It is interesting to note that both α- and β-phases are in contact with the substrate (Figure 1(a) and 2).

Discussion

The lack of a quaternary phase diagram for the (Ni-In-Ga-As) system makes it difficult to understand the phase sequences for the Ni-InGaAs intermetallic system. However, another approach could be used in order to explain the successive formation of the phases. In fact, since the In and Ga atoms are completely miscible in the zinc-blende InGaAs substrate [39–41], one can consider previous work on the ternary system (Ni-Ga-As). Extensive work has already been done on the solid-state reaction between Ni and GaAs substrates, resulting in several studies on thin films but also on bulk materials [34,42–45]. Three different ternary phase diagrams have been proposed by different researchers [36,46,47]. In fact, the proposed phase diagrams show considerable differences due to the extreme versatility of the B8 structure in which most of the phases of the system crystallize. As described by Kjekshus and Pearson [48], the B8 structure hosts two sublattices: one for the metal atoms, which can host up to two atoms, and the other for the In, Ga, and As atoms, which can also host as well, up to two atoms. Such a configuration makes the lattice very flexible in terms of site occupancy by the different atoms. In addition, the occurrence of superstructures is common and leads to short-range compositional inhomogeneity. In our case, we have used the isothermal section of the ternary phase diagram proposed by Zheng *et al.* at 600 °C [47]. In order to define the different phase compositions that we have measured, we have considered that In can occupy either As or Ga sites. Therefore, we only consider the composition of Ga, As or Ni in the measured stoichiometries of the phases (see Table 1). In Fig 4, we present an adaptation of the phase diagram proposed by Zheng *et al.* [47].

Table 1. *Summary of the measured composition of the α and β phases and the compositions without (In) for the Ni(Ga-rich) and Ni(As-rich) phases used in the ternary diagram Ni-Ga-As.*

Element	α-phase (% at.)	β-phase (fig.1 (a)) (% at.)	β'-phase (fig.1 (c)) (% at.)	Ni(Ga-rich) phase (% at.)	Ni(As-rich) phase (% at.)
Ni	62.5	52.1	52.5	62.5	52.1
Ga	27.2	4.2	3.8	28.5	4.2
As	9	31	31.7	9	43.7
In	1.3	12.7	12	-	-

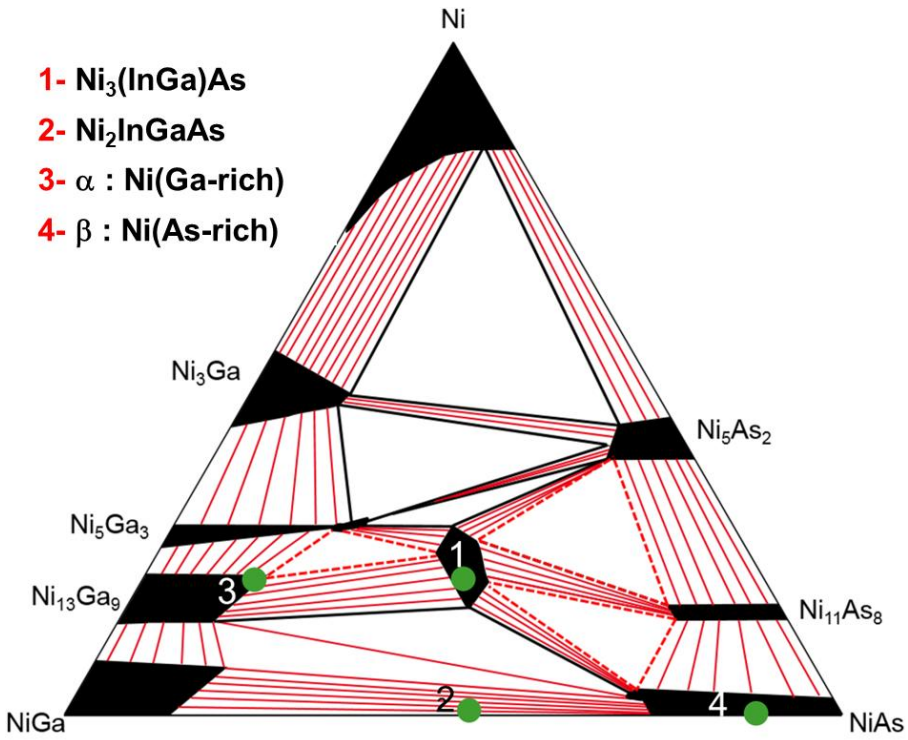

Fig 4. Ternary phase diagram adapted from Zheng *et al*. [47].

In this phase diagram, we have plotted the different possible tie lines in red. We have positioned the measured phase $Ni_3InGaAs$ from our previous work [29], and $Ni_2InGaAs$ (1 and 2, respectively), and the two phases observed in this work, α-phase and β-phase (3 and 4 respectively). The successive formation of $Ni_3InGaAs$, $Ni_2InGaAs$ and finally Ni(Ga-rich) and Ni(As-rich) phases can be explained as follows: since $Ni_3InGaAs$ is the phase with the most important formation kinetics , it is formed the first [29]. $Ni_3InGaAs$ shows a rather wide range of homogeneity in the phase diagram where Ni atoms can occupy more or less three sites in the unit lattice. At higher annealing temperatures (450 °C), $Ni_2InGaAs$ is formed, although it is not a stable phase but rather a metastable one (kinetically stable but thermodynamically unstable). If a sufficient thermal budget is applied to this phase, it can decompose into two compounds. This is the situation that we have characterized by APT after annealing at 550 °C and marked with 3 and 4 respectively on the phase diagram (Figure 4). Such phases are stable according to this phase diagram. The phase marked 3 corresponds to $Ni_{13}Ga_9$ with almost the highest As content accepted by this phase [47]. If we check the existence of a phase with In that could form a solid solution with the $Ni_{13}Ga_9$ phase, we find that the $Ni_{13}Ga_9$ and $Ni_{13}In_9$ phases [49] are complex monoclinic phases, while there is no equivalent phase with As. If such a ternary solid solution between Ni, Ga and In existed, we should have obtained a Ni(Ga, In)-rich phase with the rejection of As, which is not the case. Another hypothesis, based on the work of Guérin and Guivarc'h [46], suggests that the phase labelled as 3 is a $Ni_3Ga_{1.5}As_{0.5}$ ternary phase, which is not present in the Ni-Ga-As ternary phase diagram [35], explaining the stability of the α-phase and the rejection of In from this phase. On the other hand, to explain the stability of the β-phase, we can consider that the Ni-In-As phase diagram established is similar to that with Ga, except that the authors demonstrated the existence of a ξ-solution phase that extends on the isotherm from NiAs in the

Ni-As binary system to the binary phase ξ in the Ni-In system. Since both isotherms were carried out at the same temperature (600 °C), it is possible to speculate on the effect of the addition of In in the formation of NiAs with a low concentration of Ga (about 4%). Compared to the phases that formed in the Ni-Ga-As system, the one with In presents a greater ternary extension, probably attributed to the larger size of In atoms and the larger size of interstitial covalent radii sites when compared to Ga and As [39,41]. Therefore, it is likely that In raises a relatively high solubility in the NiAs solid solution (point 4 of the Figure 4), leading to the composition of the Ni(As-rich) phase, in equilibrium with the Ni(Ga-rich) phase, which is actually a ternary phase $Ni_3Ga_{1.5}As_{0.5}$ with a very small amount of In (1.3%). A similar system was recently studied [50] and the authors have concluded that above 450°C, $Ni_3InGaAs$ was decomposed into three phases: $Ni_xInGaAs$, NiAs and γ-Ni_3Ga_2. Based on a thinner initial metallic layer, the observed sequence could be interpreted as the more advanced state of the system observed in our case. To conclude the description, the phase in position 2 can be considered as a metastable single phase $Ni_2In_{0.5}Ga_{0.5}As$, which would be a quaternary extension of the ternary phase Ni_2GaAs found at 400 °C [30].

Conclusions

In conclusion, the reaction between the Ni film and the InGaAs substrate at 550 °C leads to in the decomposition of the intermetallic formed at high temperature allowing the formation of two new phases: α-phase and β-phase. The nature of the phases was determined by APT, and the composition was found to be $Ni_3Ga_{1.5}As_{0.5}$ and $Ni_2In_{0.52}Ga_{0.16}As_{1.32}$ for α-phase and β-phase, respectively. We found that α-phase is a Ga-rich phase and β-phase is an As-rich phase, so they can be classified as Ni(Ga-rich) and Ni(As-rich) phases, respectively. These results indicate that

since these two phases are stable in the (Ni-Ga-As) phase diagram at 550 °C, they are likely to be stable in the (Ni-Ga-As-In) quaternary system.

Acknowledgement: The authors thank M. Descoins (IM2NP) for technical support and D. Mangelink (IM2NP) for many interesting discussions.

Author contributions: N.O: Conceptualization, Investigation, Writing – original draft, Visualization; C.P: Validation, Writing – review & editing, Supervision, Visualization.; A.P: Validation, Resources, Writing – review & editing; P.R: Validation, Resources, Writing – review & editing,; L.B: Writing – review & editing,; A.B: Writing – review & editing; K.H: Conceptualization, Validation, Resources, Writing – review & editing, Project administration, Funding acquisition.

Conflicts of interest: The authors declare that they have no known competing financial interests or personal relationships that could have appeared to influence the work reported in this paper.

Data and code availability: Not Applicable.

Supplementary information: Not Applicable.

Ethical approval: Not Applicable.

Graphical Abstract

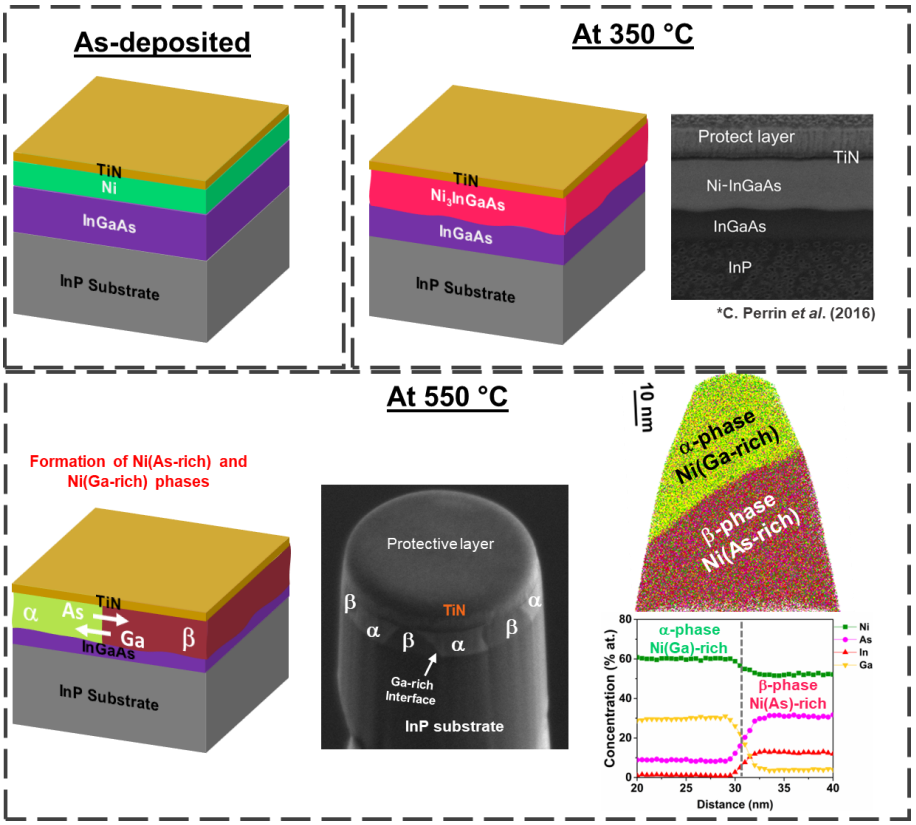
As-deposited
TiN
Ni
InGaAs
InP Substrate
At 350 °C
TiN
Ni3InGaAs
InGaAs
InP Substrate
Protect layer
TiN
Ni-InGaAs
InGaAs
InP
*C. Perrin et al. (2016)
At 550 °C
Formation of Ni(As-rich) and Ni(Ga-rich) phases
α
As
TiN
Ga
β
InGaAs
InP Substrate
Protective layer
TiN
β
α
β
α
β
α
Ga-rich Interface
InP substrate
10 nm
α-phase Ni(Ga-rich)
β-phase Ni(As-rich)
α-phase Ni(Ga)-rich
β-phase Ni(As)-rich
Concentration (% at.)
Distance (nm)
Ni
As
In
Ga

References

[1] J.A. Del Alamo, Nanometre-scale electronics with III–V compound semiconductors, Nature. 479 (2011) 317–323. https://doi.org/10.1038/nature10677.

[2] A.P. Jacob, R. Xie, M.G. Sung, L. Liebmann, R.T.P. Lee, B. Taylor, Scaling Challenges for Advanced CMOS Devices, International Journal of High Speed Electronics and Systems. 26 (2017) 1740001. https://doi.org/10.1142/S0129156417400018.

[3] D.-M. Geum, M.-S. Park, J.Y. Lim, H.-D. Yang, J.D. Song, C.Z. Kim, E. Yoon, S. Kim, W.J. Choi, Ultra-high-throughput Production of III-V/Si Wafer for Electronic and Photonic Applications, Sci Rep. 6 (2016) 20610. https://doi.org/10.1038/srep20610.

[4] C.B. Zota, C. Convertino, V. Deshpande, T. Merkle, M. Sousa, D. Caimi, L. Czomomaz, InGaAs-on-Insulator MOSFETs Featuring Scaled Logic Devices and Record RF Performance, in: 2018 IEEE Symposium on VLSI Technology, IEEE, 2018: pp. 165–166. https://doi.org/10.1109/VLSIT.2018.8510631.

[5] J.A. Del Alamo, D.A. Antoniadis, J. Lin, W. Lu, A. Vardi, X. Zhao, Nanometer-Scale III-V MOSFETs, IEEE Journal of the Electron Devices Society. 4 (2016) 205–214. https://doi.org/10.1109/JEDS.2016.2571666.

[6] C. Mukherjee, C. Raya, B. Ardouin, M. Deng, S. Fregonese, T. Zimmer, V. Nodjiadjim, M. Riet, J.-Y. Dupuy, M. Luisier, W. Quan, A. Arabhavi, C.R. Bolognesi, C. Maneux, Scalable Compact Modeling of III–V DHBTs: Prospective Figures of Merit Toward Terahertz Operation, IEEE Trans Electron Devices. 65 (2018) 5357–5364. https://doi.org/10.1109/TED.2018.2876551.

[7] J.A. Del Alamo, The High Electron Mobility Transistor, in: 75th Anniversary of the Transistor, Wiley, 2023: pp. 253–262. https://doi.org/10.1002/9781394202478.ch20.

[8] B. Szelag, K. Hassan, L. Adelmini, E. Ghegin, P. Rodriguez, F. Nemouchi, P. Brianceau, E. Vermande, A. Schembri, D. Carrara, P. Cavalie, F. Franchin, M.-C. Roure, L. Sanchez, C. Jany, S. Olivier, Hybrid III–V/Silicon Technology for Laser Integration on a 200-mm Fully CMOS-Compatible Silicon Photonics Platform, IEEE Journal of Selected Topics in Quantum Electronics. 25 (2019) 1–10. https://doi.org/10.1109/JSTQE.2019.2904445.

[9] T. Pearsall, Ga0.47In0.53As: A ternary semiconductor for photodetector applications, IEEE J Quantum Electron. 16 (1980) 709–720. https://doi.org/10.1109/JQE.1980.1070557.

[10] S. Kim, M. Yokoyama, N. Taoka, R. Iida, S. Lee, R. Nakane, Y. Urabe, N. Miyata, T. Yasuda, H. Yamada, N. Fukuhara, M. Hata, M. Takenaka, S. Takagi, Self-aligned metal source/drain InP n-metal-oxide-semiconductor field-effect transistors using Ni–InP metallic alloy, Appl Phys Lett. 98 (2011) 243501. https://doi.org/10.1063/1.3597228.

[11] Y. Chen, J. Liu, M. Zeng, F. Lu, T. Lv, Y. Chang, H. Lan, B. Wei, R. Sun, J. Gao, Z. Wang, L. Fu, Universal growth of ultra-thin III–V semiconductor single crystals, Nat Commun. 11 (2020) 3979. https://doi.org/10.1038/s41467-020-17693-5.

[12] L. Balaghi, S. Shan, I. Fotev, F. Moebus, R. Rana, T. Venanzi, R. Hübner, T. Mikolajick, H. Schneider, M. Helm, A. Pashkin, E. Dimakis, High electron mobility in strained GaAs nanowires, Nat Commun. 12 (2021) 6642. https://doi.org/10.1038/s41467-021-27006-z.

[13] X. Cai, A. Vardi, J. Grajal, J.A. del Alamo, A New Technique for Mobility Extraction in MOSFETs in the Presence of Prominent Gate Oxide Trapping: Application to InGaAs MOSFETs, IEEE Trans Electron Devices. 67 (2020) 3075–3081. https://doi.org/10.1109/TED.2020.3003844.

[14] J.M. Ramirez, H. Elfaiki, T. Verolet, C. Besancon, A. Gallet, D. Néel, K. Hassan, S. Olivier, C. Jany, S. Malhouitre, K. Gradkowski, P.E. Morrissey, P. O'Brien, C. Caillaud, N. Vaissière, J. Decobert, S. Lei, R. Enright, A. Shen, M. Achouche, III-V-on-Silicon Integration: From Hybrid Devices to Heterogeneous Photonic Integrated Circuits, IEEE Journal of Selected Topics in Quantum Electronics. 26 (2020) 1–13. https://doi.org/10.1109/JSTQE.2019.2939503.

[15] A. Guivarc'h, R. Guérin, J. Caulet, A. Poudoulec, J. Fontenille, Metallurgical study of Ni/GaAs contacts. II. Interfacial reactions of Ni thin films on (111) and (001) GaAs, J Appl Phys. 66 (1989) 2129–2136. https://doi.org/10.1063/1.344308.

[16] A. Lahav, M. Eizenberg, Y. Komem, Interfacial reactions between Ni films and GaAs, J Appl Phys. 60 (1986) 991–1001. https://doi.org/10.1063/1.337343.

[17] Ivana, Y. Lim Foo, X. Zhang, Q. Zhou, J. Pan, E. Kong, M.H. Samuel Owen, Y.-C. Yeo, Crystal structure and epitaxial relationship of $Ni_4InGaAs_2$ films formed on InGaAs by annealing, Journal of Vacuum Science & Technology B, Nanotechnology and Microelectronics: Materials, Processing, Measurement, and Phenomena. 31 (2013) 012202. https://doi.org/10.1116/1.4769266.

[18] P. Shekhter, S. Mehari, D. Ritter, M. Eizenberg, Epitaxial NiInGaAs formed by solid state reaction on $In_{0.53}Ga_{0.47}As$: Structural and chemical study, Journal of Vacuum Science & Technology B, Nanotechnology and Microelectronics: Materials, Processing, Measurement, and Phenomena. 31 (2013) 031205. https://doi.org/10.1116/1.4802917.

[19] S. Mehari, A. Gavrilov, S. Cohen, P. Shekhter, M. Eizenberg, D. Ritter, Measurement of the Schottky barrier height between Ni-InGaAs alloy and In0.53Ga0.47As, Appl Phys Lett. 101 (2012) 072103. https://doi.org/10.1063/1.4746254.

[20] S. Kim, J.D. Song, M.A. Alam, H.-J. Kim, S.K. Kim, S. Shin, J.-H. Han, D.-M. Geum, J.-P. Shim, S. Lee, H. Kim, G. Ju, Highly Stable Self-Aligned Ni-InGaAs and Non-Self-Aligned Mo Contact for Monolithic 3-D Integration of InGaAs MOSFETs, IEEE Journal of the Electron Devices Society. 7 (2019) 869–877. https://doi.org/10.1109/JEDS.2019.2907957.

[21] X. Zhang, H. Guo, X. Gong, Q. Zhou, Y.-R. Lin, H.-Y. Lin, C.-H. Ko, C.H. Wann, Y.-C. Yeo, In[sub 0.7]Ga[sub 0.3]As Channel n-MOSFET with Self-Aligned Ni–InGaAs Source and Drain, Electrochemical and Solid-State Letters. 14 (2011) H60. https://doi.org/10.1149/1.3516213.

[22] L. Czornomaz, M. El Kazzi, M. Hopstaken, D. Caimi, P. Mächler, C. Rossel, M. Bjoerk, C. Marchiori, H. Siegwart, J. Fompeyrine, CMOS compatible self-aligned S/D regions for implant-free InGaAs MOSFETs, Solid State Electron. 74 (2012) 71–76. https://doi.org/10.1016/j.sse.2012.04.014.

[23] X. Zhang, Ivana, H.X. Guo, X. Gong, Q. Zhou, Y.-C. Yeo, A Self-Aligned Ni-InGaAs Contact Technology for InGaAs Channel n-MOSFETs, J Electrochem Soc. 159 (2012) H511–H515. https://doi.org/10.1149/2.060205jes.

[24] R. Chen, S.A. Dayeh, Size and Orientation Effects on the Kinetics and Structure of Nickelide Contacts to InGaAs Fin Structures, Nano Lett. 15 (2015) 3770–3779. https://doi.org/10.1021/acs.nanolett.5b00327.

[25] S. Kim, M. Yokoyama, N. Taoka, R. Nakane, T. Yasuda, O. Ichikawa, N. Fukuhara, M. Hata, M. Takenaka, S. Takagi, Strained In $_{0.53}$ Ga $_{0.47}$ As metal-oxide-semiconductor field-effect transistors with epitaxial based biaxial strain, Appl Phys Lett. 100 (2012) 193510. https://doi.org/10.1063/1.4714770.

[26] S. Kim, M. Yokoyama, R. Nakane, O. Ichikawa, T. Osada, M. Hata, M. Takenaka, S. Takagi, Biaxially strained extremely-thin body In $_{0.53}$ Ga $_{0.47}$ As-on-insulator metal-oxide-semiconductor field-effect transistors on Si substrate and physical understanding on their electron mobility, J Appl Phys. 114 (2013) 164512. https://doi.org/10.1063/1.4828481.

[27] X. Zhang, H. Guo, H.-Y. Lin, Ivana, X. Gong, Q. Zhou, Y.-R. Lin, C.-H. Ko, C.H. Wann, Y.-C. Yeo, Reduction of Off-State Leakage Current in In0.7Ga0.3As Channel n-MOSFETs with Self-Aligned Ni-InGaAs Contact Metallization, Electrochemical and Solid-State Letters. 14 (2011) H212. https://doi.org/10.1149/1.3559754.

[28] X. Zhang, H.X. Guo, X. Gong, Y.-C. Yeo, Multiple-Gate In $_{0.53}$ Ga $_{0.47}$ As Channel n-MOSFETs with Self-Aligned Ni-InGaAs Contacts, ECS Journal of Solid State Science and Technology. 1 (2012) P82–P85. https://doi.org/10.1149/2.014202jss.

[29] C. Perrin, E. Ghegin, S. Zhiou, F. Nemouchi, P. Rodriguez, P. Gergaud, P. Maugis, D. Mangelinck, K. Hoummada, Formation of Ni3InGaAs phase in Ni/InGaAs contact at low temperature, Appl Phys Lett. 109 (2016) 1–4. https://doi.org/10.1063/1.4963132.

[30] S. Zhiou, T. Nguyen-Thanh, P. Rodriguez, F. Nemouchi, L. Rapenne, N. Blanc, N. Boudet, P. Gergaud, Reaction of Ni film with In $_{0.53}$ Ga $_{0.47}$ As: Phase formation and texture, J Appl Phys. 120 (2016) 135304. https://doi.org/10.1063/1.4963716.

[31] S. Zhiou, P. Rodriguez, F. Nemouchi, P. Gergaud, T. Nguyen-Thanh, L. Rapenne, Formation and stability of intermetallics formed by solid-state reaction of Ni on In0.53Ga0.47As, in: 2016 IEEE International Interconnect Technology Conference / Advanced Metallization Conference (IITC/AMC), IEEE, 2016: pp. 136–138. https://doi.org/10.1109/IITC-AMC.2016.7507709.

[32] S. Das, A. Sebastian, E. Pop, C.J. McClellan, A.D. Franklin, T. Grasser, T. Knobloch, Y. Illarionov, A. V. Penumatcha, J. Appenzeller, Z. Chen, W. Zhu, I. Asselberghs, L.-J. Li, U.E. Avci, N. Bhat, T.D. Anthopoulos, R. Singh, Transistors based on two-dimensional materials for future integrated circuits, Nat Electron. 4 (2021) 786–799. https://doi.org/10.1038/s41928-021-00670-1.

[33] F. Andrieu, P. Batude, L. Brunet, C. Fenouillet-Beranger, D. Lattard, S. Thuries, O. Billoint, R. Fournel, M. Vinet, A review on opportunities brought by 3D-monolithic integration for CMOS device and digital circuit, in: 2018 International Conference on IC Design & Technology (ICICDT), IEEE, 2018: pp. 141–144. https://doi.org/10.1109/ICICDT.2018.8399776.

[34] M. Ogawa, Alloying reaction in thin nickel films deposited on GaAs, Thin Solid Films. 70 (1980) 181–189. https://doi.org/10.1016/0040-6090(80)90426-5.

[35] D. Swenson, Y.A. Chang, Phase equilibria in the Ga- In- Ni system at 600 °C, Journal of Phase Equilibria. 16 (1995) 508–515. https://doi.org/10.1007/BF02646720.

[36] D.B. Ingerly, D. Swenson, C. - H. Jan, Y.A. Chang, Phase equilibria of the Ga–Ni–As ternary system, J Appl Phys. 80 (1996) 543–550. https://doi.org/10.1063/1.362758.

[37] D. Swenson, Y.A. Chang, Phase equilibria in the InNiAs system at 600°C, Materials Science and Engineering: B. 39 (1996) 232–240. https://doi.org/10.1016/0921-5107(95)01576-0.

[38] Y. Yu, C. Zhou, S. Zhang, M. Zhu, M. Wuttig, C. Scheu, D. Raabe, G.J. Snyder, B. Gault, O. Cojocaru-Mirédin, Revealing nano-chemistry at lattice defects in thermoelectric materials using atom probe tomography, Materials Today. 32 (2020) 260–274. https://doi.org/10.1016/j.mattod.2019.11.010.

[39] S. Adachi, Properties of group -IV, III-V and II-VI semi-conductors, 2005.

[40] S. Adachi, Physical Props of III-V Semicond Componds: InP, InAs, GaAs, GaP, InGaAs and InGaAsP, New York, 1992.

[41] E.K. Müller, J.L. Richards, Miscibility of III-V semiconductors studied by flash evaporation, J Appl Phys. 35 (1964) 1233–1241. https://doi.org/10.1063/1.1713600.

[42] S. Rabhi, C. Perrin-Pellegrino, S. Zhiou, M.C. Benoudia, M. Texier, K. Hoummada, Phase formation between Ni thin films and GaAs substrate, Scr Mater. 141 (2017) 28–31. https://doi.org/10.1016/j.scriptamat.2017.07.011.

[43] A. Lahav, M. Eizenberg, Y. Komem, Epitaxial Phases Formation Due to Interaction Between Ni Thin Films and GaAs, MRS Proceedings. 37 (1984). https://doi.org/10.1557/proc-37-641.

[44] A. Poudoulec, B. Guenais, A. Guivarc'h, R. Guerin, J. Caulet, M. Flohic, Transmission Electron Microscopy Study of Epitaxial Metallic Compounds on GaAs (Ni-GaAs System)., J. Appl. Phys. 43 (1988) 265–266.

[45] S. Rabhi, N. Oueldna, C. Perrin-Pellegrino, A. Portavoce, K. Kalna, M.C. Benoudia, K. Hoummada, Thickness Effect on the Solid-State Reaction of a Ni/GaAs System, Nanomaterials. 12 (2022) 2633. https://doi.org/10.3390/nano12152633.

[46] R. Guérin, A. Guivarc'h, Metallurgical study of Ni/GaAs contacts. I. Experimental determination of the solid portion of the Ni-Ga-As ternary-phase diagram, J Appl Phys. 66 (1989) 2122–2128. https://doi.org/10.1063/1.344307.

[47] X.Y. Zheng, J.C. Lin, D. Swenson, K.C. Hsieh, Y.A. Chang, Phase equilibria of GaNiAs at 600°C and the structural relationship between γ-Ni3Ga2, γ′-Ni13Ga9 and TNi3GaAs, Materials Science and Engineering B. 5 (1989) 63–72. https://doi.org/10.1016/0921-5107(89)90308-5.

[48] A. Kjekshus, W.B. Pearson, Phases with the nickel arsenide and closely-related structures, Progress in Solid State Chemistry. 1 (1964) 83–174. https://doi.org/10.1016/0079-6786(64)90004-4.

[49] K. Best, T. Gödecke, A Supplement to the System Nickel-Indium System, Z Metallkd. 60 (1969) 659–661. https://www.osti.gov/biblio/4779107 (accessed June 19, 2023).

[50] F. Boyer, K. Dabertrand, N. Bernier, C. Jany, P. Gergaud, M. Grégoire, Q. Rafhay, P. Rodriguez, Ni(Pt)-based CMOS-compatible contacts on p-InGaAs for III–V photonic devices, Mater Sci Semicond Process. 154 (2023) 107199. https://doi.org/10.1016/j.mssp.2022.107199.